ChemComm

COMMUNICATION

View Article Online
View Journal | View Issue

Cite this: *Chem. Commun.*, 2022, 58, 3134

Received 6th January 2022,
Accepted 9th February 2022

DOI: 10.1039/d1cc07303f

rsc.li/chemcomm

AuB_8^-: an Au–borozene complex†

Wei-Jia Chen,‡[a] Yang-Yang Zhang,‡[b] Wan-Lu Li,[b] Hyun Wook Choi,[a] Jun Li *[bc] and Lai-Sheng Wang *[a]

Photoelectron spectroscopy and quantum chemistry studies are used to investigate the structure and bonding of AuB_8^-. Global minimum sturctural searches show that AuB_8^- possesses a chair-like structure, which can be viewed as Au^+ bonded to the edge of the doubly-aromatic B_8^{2-} borozene, $Au^+[\eta^2\text{-}B_8^{2-}]$. Chemical bonding analyses reveal that the AuB_8^- is a novel borozene complex with unique Au–borozene bonding.

The electron deficiency of boron leads to unique structures and interesting bonding in both boron compounds and bulk boron allotropes.[1–3] Over the past two decades, extensive research has been done on a wide range of size-selected boron clusters using joint photoelectron spectroscopy (PES) and quantum chemical calculations,[4–7] as well as ion mobility and infrared spectroscopy.[8,9] In contrast to bulk boron, small boron clusters are found to possess two-dimensional (2D) structures consisting of B_3 triangles decorated with tetragonal, pentagonal, and hexagonal holes.[5–7] The 2D structures are stabilized by σ and π electron delocalization to accommodate boron's electron deficiency in finite sizes.[10,11] One of the most important findings among the 2D boron clusters is the B_{36} cluster, which contains a central hexagonal vacancy and provides the first experimental evidence about the viability of atom-thin 2D borons (a.k.a. borophenes).[12] Atom-thin 2D borons stabilized by hexagonal holes were first predicted to be stable by theoretical calculations[13,14] and borophenes have been synthesized on metal substrates,[15,16] becoming an important class of synthetic 2D materials.[17] Another interesting finding is the B_{40} cluster, the first all-boron fullerene.[18] The B_{48}^- cluster is the largest boron cluster that has been characterized experimentally heretofore and found to possess a bilayer structure.[19] Recently, bilayer borophenes have also been successfully synthesized on Ag and Cu surfaces.[20,21]

The B_7^-, B_8^-, and B_9^- series were among the first few size-selected boron clusters to be characterized by PES and quantum calculations.[22,23] The B_7^- cluster was found to have a C_{6v} ($^3A_1$) structure with σ and π double aromaticity. The closed-shell doubly aromatic B_7^{3-} was first realized in the half-sandwich AlB_7 and PrB_7 clusters.[24,25] The B_9^- cluster was found to have a closed-shell D_{7h} ($^1A_{1g}$) structure with double aromaticity and its unique structure and bonding inspired the designs and syntheses of a class of metal-centred borometallic species $M©B_n^-$.[26] The B_8^- cluster was first found to have a C_{2v} ($^2B_1$) structure, whereas the doubly aromatic closed-shell B_8^{2-} was realized in the LiB_8^- charge-transfer complex.[27] In a recent study on a series of lanthanide (Ln) octa-boron clusters (LnB_8^-), it is recognized that the B_7^{3-}, B_8^{2-}, and B_9^- series of closed-shell clusters are analogous in their π aromaticity and their trends of size and charge to the prototypical aromatic hydrocarbons, $C_5H_5^-$, C_6H_6, and $C_7H_7^+$, respectively, and a name "borozene" is thereoff proposed for these $4n + 2$ π-electron aromatic boron clusters.[28] The B_8^{2-} borozene is particularly interesting due to its perfect planarity and high stability. It has been found that it can form charge-transfer complexes with elements of low electronegativities,[27–33] leading to the realization of monovalent lanthanides in the LnB_8^- (*i.e.*, $Ln^+[\eta^8\text{-}B_8^{2-}]$) half-sandwich complexes.[28] However, for transition-metal MB_8^- species it has been found that metal-centred B_8 monocyclic ring structures ($M©B_8$) dominate due to the favourable in-plane d–p π interactions.[26] On the other hand, in a recent study of BiB_8 it is found that the Bi atom is bonded on the surface of the B_8^{2-} borozene off centre due to the 6p-π interaction between Bi and B_8.[34] In the current study, we investigate the AuB_8^- cluster to explore the bonding mode

[a] *Department of Chemistry, Brown University, Providence, RI 02912, USA. E-mail: lai-sheng_wang@brown.edu*
[b] *Department of Chemistry and Key Laboratory of Organic Optoelectronics & Molecular Engineering of Ministry of Education, Tsinghua University, Beijing 100084, China. E-mail: junli@tsinghua.edu.cn*
[c] *Department of Chemistry, Southern University of Science and Technology, Shenzhen 518055, China*

† Electronic supplementary information (ESI) available: Additional theoretical data and analyses. See DOI: 10.1039/d1cc07303f

‡ These authors contributed equally.

between Au and borozene. Gold is a monovalent element, does it form a C_{8v} AuB_8^- charge-transfer complex? Due to the strong relativistic effects,[35] Au has been found to form strong covalent bonding with main group elements[36] and display H-like bonding properties with boron.[37–40] The $H_2B_8^-$ species was found to be an elongated double chair structure with two terminal B–H bonds.[41] Does the Au–B covalent bonding distort the borozene into a similar double chain structure with a terminal Au–B bond?

We have produced AuB_8^- using a laser vaporization cluster source and combined PES with quantum chemistry to elucidate its structure and bonding. Vibrationally-resolved photoelectron spectra are obtained and the electron affinity of AuB_8 is measured to be 2.96 ± 0.0 3 eV. The global minimum of AuB_8^- is found to consist of a gold atom bonded on the edge of a planar B_8 motif in a chair-like structure, which can be viewed as an Au–borozene complex, $Au^+[\eta^2\text{-}B_8^{2-}]$. The elongated double-chain structure with a terminal Au atom is a high energy isomer, whereas the high-symmetry C_{7v} half-sandwich structure is not stable. Both ionic bonding and $5d_\pi$-π interactions between Au^+ and B_8^{2-} favour the bidentate chair-like structure.

The photoelectron spectra of AuB_8^- at three photon energies are shown in Fig. 1. These spectra are well resolved with distinct photodetachment transitions and even vibrational structures. The 355 nm spectrum (Fig. 1a) displays one vibrationally-resolved band (X), consisting of two vibrational progressions with frequencies of ~480 cm^{-1} and ~1450 cm^{-1}, respectively (Fig. 1d). The 0–0 transition is the most intense vibrational peak, defining a VDE of 3.00 eV. The 0–0 vibrational peak appeared broader than the instrumental resolution and it might contain unresolved low-frequency vibrational features. Using the leading edge of the 0–0 peak, we evaluated an ADE of 2.96 eV, which also represents the electron affinity (EA) of AuB_8. Two more PES bands are resolved at 266 nm (Fig. 1b), including a broad band A centred at 3.88 eV and a sharp peak near the threshold at 4.63 eV, which is the 0–0 transition of a short vibrational progression for band B, as shown at 193 nm (Fig. 1c). The vibrational spacing was estimated to be ~1050 cm^{-1}. Band B is closely followed by a broader band C at 4.94 eV. Two more bands at higher binding energies, a sharp band D and a broader band E, are clearly resolved at 5.65 eV and 6.07 eV, respectively. The binding energies of all the observed PES bands, are given in Table 1, where they are compared with the theoretical results.

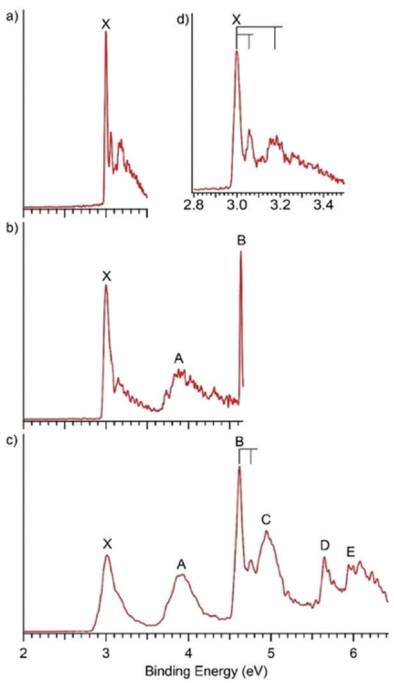

Fig. 1 Photoelectron spectra of AuB_8^- at (a) 355 nm (3.496 eV), (b) 266 nm (4.661 eV) and (c) 193 nm (6.424 eV). An expanded view of the X band is given in (d) to show the resolved vibrational features.

Extensive GM searches were carried out for AuB_8^- and AuB_8 using the TGMin code.[42,43] The three lowest-lying structures are shown in Fig. 2 at three levels of theory and more higher-lying isomers at the PBE/TZP level are given in Fig. S1 and S2 (ESI†) for AuB_8^- and AuB_8, respectively. The GM search revealed a closed-shell chair-like C_s ($^1A'$) structure for AuB_8^-, consisting of a gold atom bonded out-of-plane on the edge of a planar B_8 motif (Fig. 2a), which is similar to the D_{7h} GM structure of bare B_8.[23] The closed-shell C_s ($^1A'$) structure was found to be significantly more stable than LM1 at all three levels of theory. The LM1 (C_s, $^1A'$) of AuB_8^- was 13.15 kcal mol^{-1} higher in energy than the GM at the DLPNO-CCSD(T) level. The B_8 unit in LM1 consists a B atom bonded to the edge of a B-centred hexagonal B_7 motif. The LM2 (C_s, $^1A'$) of AuB_8^- consists of a double-chain B_8 motif, which is 14.52 kcal mol^{-1} higher in energy than the GM at the DLPNO-CCSD(T) level. The spin-doublet GM of neutral AuB_8 ($^2A'$) is similar to that of the anion (Fig. 2b). There is relatively little structural change upon detachment of an electron from AuB_8^-, as compared in Fig. S3 (ESI†). A similar AuB_8 structure was suggested in a recent computational study of transition metal doped boron clusters.[44] The LM1 and LM2 of AuB_8 are also similar to those of the anion, but their stabilities are switched. Both LM1 and LM2 of AuB_8 are significantly higher in energy than the GM at all three levels of theory.

The first ADE/VDE for the GM of AuB_8^- were calculated at the PBE and PBE0 levels of theory, as shown in Table S1 (ESI†). The computed first ADE/VDE of 2.91/2.97 eV at the PBE level are in agreement with the experimental results of 2.96/3.00 eV, whereas the PBE0 values are lower in general. The HOMO (8a″)

Table 1 The experimental vertical detachment energies (VDEs) in eV of AuB_8^- in comparison with theoretical VDEs computed for the global minimum C_s ($^1A'$) structure at the TD-SAOP/TZP level

Band	VDE (exp)[a]	Final state and electron configuration	VDE (theo.)
X	3.00	$^2A'\{\ldots 6a''^2 12a'^2 13a'^2 7a''^2 14a'^2 \mathbf{8a''^1}\}$	2.97
A	3.88	$^2A'\{\ldots 6a''^2 12a'^2 13a'^2 7a''^2 \mathbf{14a'^1} 8a''^2\}$	3.92
B	4.63	$^2A'\{\ldots 6a''^2 12a'^2 13a'^2 \mathbf{7a''^1} 14a'^2 8a''^2\}$	4.67
C	4.94	$^2A'\{\ldots 6a''^2 12a'^2 \mathbf{13a'^1} 7a''^2 14a'^2 8a''^2\}$	5.04
D	5.65	$^2A'\{\ldots 6a''^2 \mathbf{12a'^1} 13a'^2 7a''^2 14a'^2 8a''^2\}$	5.72
E	6.07	$^2A'\{\ldots \mathbf{6a''^1} 12a'^2 13a'^2 7a''^2 14a'^2 8a''^2\}$	6.09

[a] The experimental uncertainty was estimated to be ±0.03 eV.

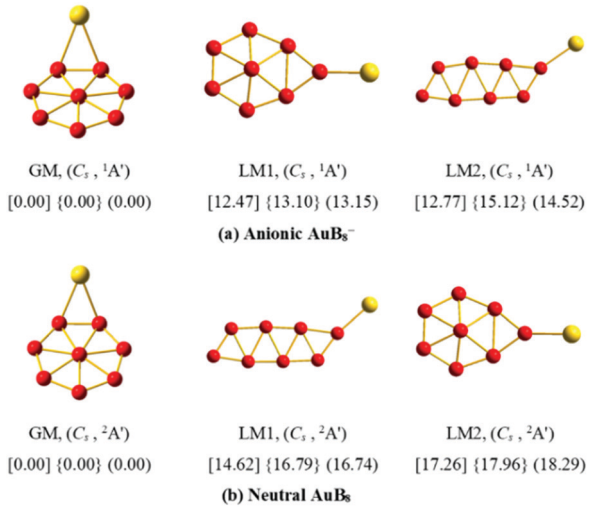

Fig. 2 The structures and relative energies of the global minimum (GM) and two low-lying isomers (LMs) for (a) AuB_8^- and (b) AuB_8. The relative energies (in kcal mol^{-1}) calculated at the SR-ZORA PBE/TZP and PBE0/TZP level are given in the square brackets and braces, respectively. The single-point DLPNO-CCSD(T)/Def2-TZVP energies are given in the regular parentheses. The coordinates of these structures are given in the ESI† (Table S3).

of AuB_8^- is a π orbital on the B_8 moiety (Fig. 3). The small bond length changes between the anion and the neutral (Fig. S3, ESI†) are consistent with the nature of this MO. We also computed the vibrational frequencies for AuB_8 to help interpret the observed vibrational progressions of the ground state detachment transition, as given in Fig. S4 (ESI†). Because the symmetries of the anion and neutral are the same, only totally symmetric modes are allowed. The lower frequency mode (480 cm^{-1}) should correspond to the ν_6(A′) mode mainly involving the B_2–Au stretching. The computed frequency of 475 cm^{-1} (Fig. S4, ESI†) agrees well with the experimental result. The observed high frequency mode (1450 cm^{-1}) should correspond to the ν_{12}(A′) B–B stretching mode. The computed frequency of 1339 cm^{-1} appeared to be lower than the experimental value, mainly due to the large uncertainty in the experimental measurement.

The calculated VDE from HOMO−1 (14a′) is 3.92 eV, in good agreement with the measured VDE of band A (Table 1). The 14a′ orbital (Fig. 3) involves π bonding between the B_8 moiety and the Au atom. Detachment of an electron from the 14a′ orbital is expected to induce low-frequency vibrations involving both B–Au stretching and bending motions, consistent with the broad and unresolved band A (Fig. 1). The computed VDEs for the HOMO−2 (7a″), HOMO−3 (13a′), HOMO−4 (12a′), and HOMO−5 (6a″) are all in good agreement with the measured VDEs for bands B, C, D, and E, respectively (Table 1). The closed-shell nature of AuB_8^- greatly simplifies the observed spectrum, because each occupied MO gives rise to only one detachment channel. A simulated spectrum was obtained by fitting each computed VDE with a Gaussian of 0.1 eV width, as compared with the 193 nm spectrum in Fig. S5 (ESI†). For comparison, simulated spectra from LM1 and LM2 of AuB_8^- are also included in Fig. S5 (ESI†), but they clearly do not agree with the observed spectrum. The excellent agreement between the experimental and theoretical results firmly confirms the chair-like C_s structure as the global minimum of AuB_8^-.

We used the AdNDP approach to analyse the chemical bonds in AuB_8^-. AdNDP transforms MOs into semi-localized bonding units, providing a more intuitive view of multi-centred chemical bonding for complicated molecular systems.[45–47] The AdNDP results of AuB_8^- are displayed in Fig. 4, showing seven two-centre two-electron (2c–2e) B–B σ bonds on the periphery of the B_8 moiety, three 8c–2e σ bonds, and three 9c–2e π bonds, in addition to the five 5d-based lone pairs. The occupation number (ON) of some 5d lone pairs is less than 2, indicating participation of the 5d orbitals in bonding with the B_8 moiety. The delocalized σ and π bonding electrons fulfil the 4n + 2 rule, respectively, giving rise to double aromaticity, even though two of the π bonds describe bonding with the Au atom. The Nucleus Independent Chemical Shifts (NICS) of AuB_8^- are also calculated (Fig. S6, ESI†), which provides another support for its double aromaticity.

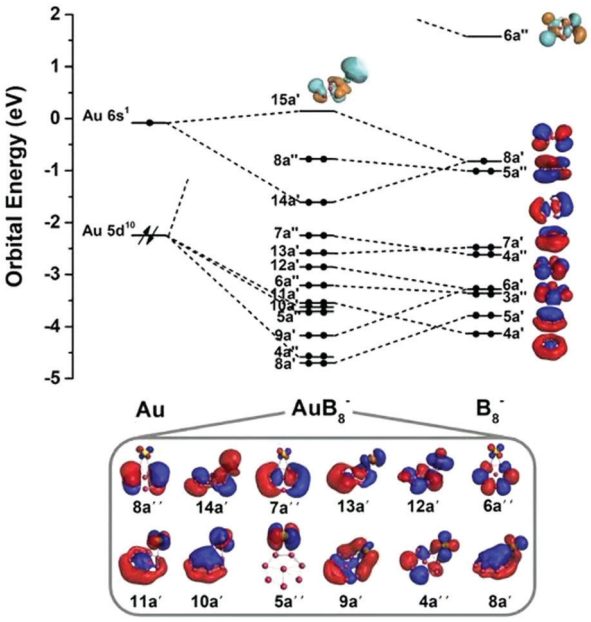

Fig. 3 Kohn–Sham molecular orbitals (MOs) of AuB_8^- (bottom) and the MO energy-level correlation diagram (top) between Au and B_8^- at the PBE/TZP level. The double arrow indicates the 5d^{10} shell of Au. (Isovalue = 0.03 a.u.).

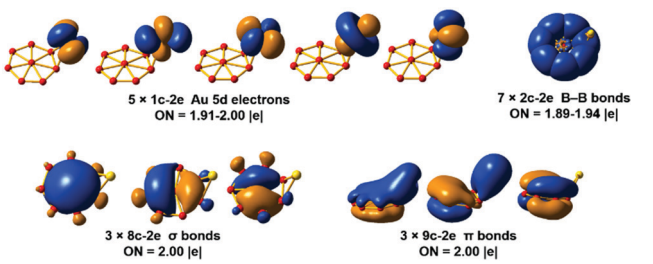

Fig. 4 AdNDP analyses for AuB_8^- at the B3LYP/LANL2DZ/6-311G* level. ON denotes occupation number. (Isovalue = 0.03 a.u.).

To better understand the stability of AuB_8^-, we calculated its bond dissociation energies (BDEs). The BDE for the three dissociation channels calculated at the B3LYP/Lanl2DZ/6-311 + G(d) level are:

$$AuB_8^- (C_s, {}^1A') \rightarrow Au ({}^2\Sigma_g^+) + B_8^- (C_s, {}^2A') \quad 2.24 \text{ eV} \quad (1)$$

$$AuB_8^- (C_s, {}^1A') \rightarrow Au^- ({}^1\Sigma_g^+) + B_8 (C_s, {}^1A') \quad 3.48 \text{ eV} \quad (2)$$

$$AuB_8^- (C_s, {}^1A') \rightarrow Au^+ ({}^1\Sigma_g^+) + B_8^{2-} (C_s, {}^1A') \quad 13.63 \text{ eV} \quad (3)$$

The remarkable BDE of 13.63 eV for channel (3) suggests AuB_8^- is more suitable to be viewed as $Au^+[\eta^2\text{-}B_8^{2-}]$, *i.e.*, an Au–borozene complex. The charge analyses for AuB_8^- using different methods (Table S2, ESI†) support this formulation. The B–Au distances between the gold atom and the coordinated boron atoms in AuB_8^- are 2.20 Å, which is larger than the Au–B single-bond length of 2.09 Å based on the self-consistent covalent radii of Pyykkö.[48] Thus, the Au–B bonding is relatively weak in the Au–borozene complex, deriving mainly from the delocalized Au $5d_\pi$ and B_8 π bonding (Fig. 4). The remarkable stability of the gold–borozene complex is due to both covalent and ionic interactions between Au^+ and the doubly aromatic B_8^{2-}. Thus, the structure and bonding in the Au–borozene complex are quite different from those of the recently reported LnB_8^- lanthanide complexes.[28] The Ln–borozene complexes form half-sandwich structures featuring the rare monovalent Ln(I) centres because of strong ionic bonding. Both covalent and ionic bonding in the Au^+–B_8^{2-} borozene complex favours the chair-like structure for AuB_8^-.

Clearly, the structures of the MB_8 species depend on the nature of the M–B_8 interactions and the size of the metal atom. Whether the borozene complex exist for MB_8 is determined by the metal. Transition metals with strong in-plane d_π-π bonding tend to form metal-centred borometallic wheels (M©B_8).[26] Elements with low electronegativities, such as the alkalis, alkali earths, rare earths or aluminium favour half-sandwich borozene complexes, $M^+[\eta^8\text{-}B_8^{2-}]$, due to strong M–borozene ionic bonding.[27–33] For intermediate cases where both ionic and covalent bonding exist, such as BiB_8 and AuB_8^-, the metal atom tends to be off centre in the M–borozene complexes. In BiB_8, the strong 6p-π covalent interactions yield a pentadentate borozene complex, $Bi^{2+}[\eta^5\text{-}B_8^{2-}]$,[34] whereas AuB_8^- is a bidentate complex $Au^+[\eta^2\text{-}B_8^{2-}]$, due to the weak $5d_\pi$-π interactions.

In conclusion, we have produced and investigated the AuB_8^- cluster to assess the feasibility of Au–borozene complexes. Well-resolved photoelectron spectra are used to confirm the global minimum of AuB_8^- as a closed-shell chair-like Au–borozene complex, $Au^+[\eta^2\text{-}B_8^{2-}]$. This unique structure is due to both ionic and $5d_\pi$-π covalent bonding between Au^+ and the doubly aromatic B_8^{2-} borozene. A variety of structures are possible for the M–B_8 borozene complexes, depending on the metal dopant and the nature of the M–B_8 bonding. Investigations of metal–borozene complexes will help us develop a better understanding of metal–boron bonding, as well as providing valuable information about the feasibility to use borozenes as new aromatic ligands to synthesize novel boron compounds.

The experiment was supported by the National Science Foundation (CHE-2053541 to L. S. W.). J. L. was supported by the National Natural Science Foundation of China (Grant 22033005) and the Guangdong Provincial Key Laboratory of Catalysis (No. 2020B121201002). Computational resources are supported by the Center for Computational Science and Engineering (SUSTech).

Conflicts of interest

There are no conflicts to declare.

Notes and references

1 W. N. Lipscomb, *Science*, 1977, **196**, 1047–1055.
2 B. Albert and H. Hillebrecht, *Angew. Chem., Int. Ed.*, 2009, **48**, 8640–8668.
3 A. R. Oganov, *et al.*, *Nature*, 2009, **457**, 863–867.
4 A. N. Alexandrova, *et al.*, *Coord. Chem. Rev.*, 2006, **250**, 2811–2866.
5 A. P. Sergeeva, *et al.*, *Acc. Chem. Res.*, 2014, **47**, 1349–1358.
6 L. S. Wang, *Int. Rev. Phys. Chem.*, 2016, **35**, 69–142.
7 T. Jian, *et al.*, *Chem. Soc. Rev.*, 2019, **48**, 3550–3591.
8 E. Oger, *et al.*, *Angew. Chem., Int. Ed.*, 2007, **46**, 8503–8506.
9 S. Pan, *et al.*, *Acc. Chem. Res.*, 2019, **52**, 2732–2744.
10 H. J. Zhai, *et al.*, *Nat. Mater.*, 2003, **2**, 827–833.
11 A. I. Boldyrev and L. S. Wang, *Phys. Chem. Chem. Phys.*, 2016, **18**, 11589–11605.
12 Z. A. Piazza, *et al.*, *Nat. Commun.*, 2014, **5**, 3113.
13 H. Tang and S. Ismail-Beigi, *Phys. Rev. Lett.*, 2007, **99**, 115501.
14 X. Yang, *et al.*, *Phys. Rev. B: Condens. Matter Mater. Phys.*, 2008, **77**, 041402.
15 A. J. Mannix, *et al.*, *Science*, 2015, **350**, 1513.
16 B. Feng, *et al.*, *Nat. Chem.*, 2016, **8**, 563–568.
17 S.-Y. Xie, *et al.*, *Adv. Mater.*, 2019, **31**, 1900392.
18 H. J. Zhai, *et al.*, *Nat. Chem.*, 2014, **6**, 727–731.
19 W. J. Chen, *et al.*, *Nanoscale*, 2021, **13**, 3868–3876.
20 X. Liu, *et al.*, *Nat. Mater.*, 2021, **21**, 35–40.
21 C. Chen, *et al.*, *Nat. Chem.*, 2022, **14**, 25–31.
22 A. N. Alexandrova, *et al.*, *J. Phys. Chem. A*, 2004, **108**, 3509–3517.
23 H. J. Zhai, *et al.*, *Angew. Chem., Int. Ed.*, 2003, **42**, 6004–6008.
24 T. R. Galeev, *et al.*, *J. Chem. Phys.*, 2011, **135**, 104301.
25 T. T. Chen, *et al.*, *Angew. Chem., Int. Ed.*, 2017, **56**, 6916–6920.
26 C. Romanescu, *et al.*, *Acc. Chem. Res.*, 2013, **46**, 350–358.
27 A. N. Alexandrova, *et al.*, *Inorg. Chem.*, 2004, **43**, 3552–3554.
28 W. L. Li, *et al.*, *Nat. Commun.*, 2021, **12**, 6467.
29 T. B. Tai and M. T. Nguyen, *Chem. Phys.*, 2010, **375**, 35–45.
30 Y. Liao, *et al.*, *Phys. Chem. Chem. Phys.*, 2012, **14**, 14898–14904.
31 J. Gu, *et al.*, *Comput. Theor. Chem.*, 2014, **1049**, 67–74.
32 A. C. Reber and S. N. Khanna, *J. Chem. Phys.*, 2015, **142**, 054304.
33 R. Yu, *et al.*, *Phys. Chem. Chem. Phys.*, 2020, **22**, 12312–12320.
34 W. J. Chen, *et al.*, *J. Phys. Chem. A*, 2021, **125**, 6751–6760.
35 P. Pyykko, *Chem. Rev.*, 1988, **88**, 563–594.
36 L. S. Wang, *Phys. Chem. Chem. Phys.*, 2010, **12**, 8694–8705.
37 D. Y. Zubarev, *et al.*, *Inorg. Chem.*, 2006, **45**, 5269–5271.
38 H. J. Zhai, *et al.*, *J. Phys. Chem. A*, 2006, **110**, 1689–1693.
39 Q. Chen, *et al.*, *J. Chem. Phys.*, 2013, **138**, 084306.
40 P. Shao, *et al.*, *RSC Adv.*, 2015, **5**, 87855–87863.
41 W. L. Li, *et al.*, *J. Am. Chem. Soc.*, 2012, **134**, 13228–13231.
42 Y. F. Zhao, *et al.*, *Nano Res.*, 2017, **10**, 3407–3420.
43 X. Chen, *et al.*, *J. Comput. Chem.*, 2019, **40**, 1105–1112.
44 X. Wu, *et al.*, *Eur. Phys. J. Plus*, 2021, **136**, 328.
45 D. Y. Zubarev and A. I. Boldyrev, *Phys. Chem. Chem. Phys.*, 2008, **10**, 5207–5217.
46 D. Y. Zubarev and A. I. Boldyrev, *J. Org. Chem.*, 2008, **73**, 9251–9258.
47 N. V. Tkachenko and A. I. Boldyrev, *Phys. Chem. Chem. Phys.*, 2019, **21**, 9590–9596.
48 P. Pyykko, *J. Phys. Chem. A*, 2015, **119**, 2326–2337.